

Comparative analysis of the semileptonic $\Lambda_b \rightarrow \Lambda \ell^+ \ell^-$ transition in SM and different SUSY scenarios using form factors from full QCD

K. Azizi^{1 *}, S. Kartal^{2 †}, A. T. Olgun^{2 ‡}, Z. Tavukoğlu^{2 §}

¹ Department of Physics, Doğuş University, Acıbadem-Kadıköy, 34722 İstanbul, Turkey

² Department of Physics, İstanbul University, Vezneciler, 34134 İstanbul, Turkey

Abstract

We work out the semileptonic $\Lambda_b \rightarrow \Lambda \ell^+ \ell^-$ transition in standard as well as different supersymmetric models. In particular, considering the parametrization of the matrix elements entered the low energy effective Hamiltonian in terms of form factors in full QCD, we calculate the amplitude and differential decay rate responsible for this decay channel in supersymmetric models. We then use the form factors calculated via light cone QCD sum rules in full theory to analyze the differential branching ratio and lepton forward-backward asymmetry of this decay channel in different supersymmetric models and compare the obtained results with those of the standard model. We also discuss how the results of different supersymmetric models deviate from the standard model predictions and which SUSY scenarios are favored.

PACS number(s): 12.60.-i, 12.60.Jv, 13.30.-a, 13.30.Ce, 14.20.Mr

*e-mail: kazizi@dogus.edu.tr

†e-mail: sehban@istanbul.edu.tr

‡e-mail: a.t.olgun@gmail.com

§e-mail: z.tavukoglu@gmail.com

1 Introduction

Recently, there has been an important progress on the course of searching for Higgs boson as a missing ingredient of the standard model (SM). The ATLAS and CMS Collaborations at CERN reported their observation on a Higgs-like particle with a statistical significance of 5σ [1]. Now, it is searched whether this Higgs-like boson is the standard or non-standard Higgs particle. The supersymmetry (SUSY) has been the most popular paradigm for new physics (NP) scenarios in the last decades. The recent progresses have stimulated the theoretical works dedicated to the study of how a relatively heavy Higgs constrains the parameters of SUSY (for a discussion see for instance [2]). On the other hand, with these developments, we hope that we will have an experimental progress in searching for SUSY particles both directly by increasing the center of mass energy and indirectly by studying the flavor changing neutral current (FCNC) transitions.

In the present work, we theoretically analyze the semileptonic FCNC decay of the $\Lambda_b \rightarrow \Lambda \ell^+ \ell^-$ in existing related different supersymmetric models. In principle, the SUSY particles can contribute to such loop level transitions. Hence, we look for the effect of superparticles in this channel via calculating some related observables like differential branching ratio and lepton forward-backward asymmetry (FBA). Due to the specific features, there are different SUSY scenarios such as SUSY I, SUSY II, SUSY III and SUSY SO(10) [3–6]. In these models, the Wilson coefficients receive contributions from neutral Higgs bosons (NHBs) that are proportional to $\tan^3\beta$, where $\tan\beta$ has been defined as the ratio of the vacuum expectation values of two neutral Higgs bosons (h^0, A^0). According to the $\tan\beta$ and an extra parameter μ with dimension of mass corresponding to mass term mixing of two Higgs doublets, the different SUSY models are categorized. In SUSY I, the μ takes negative value, some of the Wilson coefficients change their signs and the contributions of NHBs have been neglected. In SUSY II, the $\tan\beta$ takes large value while masses of the superparticles are small in order of a few hundred GeV. In SUSY III, the $\tan\beta$ is large and the masses of the superparticles are relatively large up to 450 GeV or more. In SUSY SO(10) model, the imaginary parts of the Wilson coefficients are large and the NHBs contributions are considered.

In the last year, the CDF Collaboration at Fermilab [7] has reported the first observation on the baryonic FCNC transition of $\Lambda_b^0 \rightarrow \Lambda \mu^+ \mu^-$ with 24 signal events and statistical of 5.8 deviations. They have measured a branching ratio of $[1.73 \pm 0.42(stat) \pm 0.55(syst)] \times 10^{-6}$. This decay channel is in the focus of different experiments like LHCb at CERN [8]. Hence, theoretical and phenomenological predictions on the observables defining this channel can

help us in the course of searching indirectly for SUSY particles in this stage. Comparison of different theoretical results with experimental data may help us get useful informations about the existence of the SUSY particles. Note that the rare $\Lambda_b \rightarrow \Lambda \ell^+ \ell^-$ transition was analyzed in the same frameworks in [5] using only two form factors calculated via heavy quark effective theory (HQET). In this work, we generalize those calculations to include all form factors in full theory.

In the next section, introducing the effective Hamiltonian both in the SM and SUSY models, we calculate the amplitude of the decay under consideration in terms of twelve form factors enrolled to the transition matrix elements. In section 3, we calculate the formula for the differential decay rate in SUSY and numerically analyze it together with the branching ratio and lepton FBA. We also compare the obtained results on the considered physical quantities in different SUSY models with those obtained from the SM. The last section encompasses our concluding remarks.

2 The effective Hamiltonian and transition matrix elements

In the SM, the $\Lambda_b \rightarrow \Lambda \ell^+ \ell^-$ transition goes with the $b \rightarrow s \ell^+ \ell^-$ at quark level whose effective Hamiltonian is given by

$$\begin{aligned} \mathcal{H}^{eff} = & \frac{G_F \alpha_{em} V_{tb} V_{ts}^*}{2\sqrt{2}\pi} \left[C_9^{eff} \bar{s} \gamma_\mu (1 - \gamma_5) b \bar{\ell} \gamma^\mu \ell + C_{10} \bar{s} \gamma_\mu (1 - \gamma_5) b \bar{\ell} \gamma^\mu \gamma_5 \ell \right. \\ & \left. - 2m_b C_7^{eff} \frac{1}{q^2} \bar{s} i \sigma_{\mu\nu} q^\nu (1 + \gamma_5) b \bar{\ell} \gamma^\mu \ell \right], \end{aligned} \quad (2.1)$$

where G_F is the Fermi coupling constant, α_{em} is the fine structure constant at Z mass scale, V_{ij} are elements of the Cabibbo-Kobayashi-Maskawa (CKM) matrix; and the C_7^{eff} , C_9^{eff} and C_{10} are the Wilson coefficients. Considering the contributions of the new operators coming from the new interactions induced by the NHBs exchanged diagrams, the supersymmetric

effective Hamiltonian can be written as

$$\begin{aligned}
\mathcal{H}_{SUSY}^{eff} = & \frac{G_F \alpha_{em} V_{tb} V_{ts}^*}{2\sqrt{2}\pi} \left[C_9^{eff} \bar{s} \gamma_\mu (1 - \gamma_5) b \bar{\ell} \gamma^\mu \ell + C_9'^{eff} \bar{s} \gamma_\mu (1 + \gamma_5) b \bar{\ell} \gamma^\mu \ell \right. \\
& + C_{10} \bar{s} \gamma_\mu (1 - \gamma_5) b \bar{\ell} \gamma^\mu \gamma_5 \ell + C_{10}' \bar{s} \gamma_\mu (1 + \gamma_5) b \bar{\ell} \gamma^\mu \gamma_5 \ell \\
& - 2m_b C_7^{eff} \frac{1}{q^2} \bar{s} i \sigma_{\mu\nu} q^\nu (1 + \gamma_5) b \bar{\ell} \gamma^\mu \ell - 2m_b C_7'^{eff} \frac{1}{q^2} \bar{s} i \sigma_{\mu\nu} q^\nu (1 - \gamma_5) b \bar{\ell} \gamma^\mu \ell \\
& + C_{Q_1} \bar{s} (1 + \gamma_5) b \bar{\ell} \ell + C_{Q_1}' \bar{s} (1 - \gamma_5) b \bar{\ell} \ell \\
& \left. + C_{Q_2} \bar{s} (1 + \gamma_5) b \bar{\ell} \gamma_5 \ell + C_{Q_2}' \bar{s} (1 - \gamma_5) b \bar{\ell} \gamma_5 \ell \right], \tag{2.2}
\end{aligned}$$

where the new Wilson coefficients, C_{Q_1} and C_{Q_2} exist in the all considered SUSY models, while the primed coefficients only appear in SUSY SO(10) scenario.

The amplitude is obtained by sandwiching the new effective Hamiltonian between the initial and final baryonic states, i.e.,

$$\mathcal{M}_{SUSY}^{\Lambda_b \rightarrow \Lambda \ell^+ \ell^-} = \langle \Lambda(p_\Lambda) | \mathcal{H}_{SUSY}^{eff} | \Lambda_b(p_{\Lambda_b}) \rangle, \tag{2.3}$$

where p_{Λ_b} and p_Λ are momenta of the Λ_b and Λ baryons, respectively. To proceed, we need to calculate the following matrix elements parametrized in terms of twelve form factors in full theory:

$$\begin{aligned}
\langle \Lambda(p_\Lambda) | \bar{s} \gamma_\mu (1 - \gamma_5) b | \Lambda_b(p_{\Lambda_b}) \rangle = & \bar{u}_\Lambda(p_\Lambda) \left[\gamma_\mu f_1(q^2) + i \sigma_{\mu\nu} q^\nu f_2(q^2) + q^\mu f_3(q^2) \right. \\
& \left. - \gamma_\mu \gamma_5 g_1(q^2) - i \sigma_{\mu\nu} \gamma_5 q^\nu g_2(q^2) - q^\mu \gamma_5 g_3(q^2) \right] u_{\Lambda_b}(p_{\Lambda_b}), \tag{2.4}
\end{aligned}$$

$$\begin{aligned}
\langle \Lambda(p_\Lambda) | \bar{s} \gamma_\mu (1 + \gamma_5) b | \Lambda_b(p_{\Lambda_b}) \rangle = & \bar{u}_\Lambda(p_\Lambda) \left[\gamma_\mu f_1(q^2) + i \sigma_{\mu\nu} q^\nu f_2(q^2) + q^\mu f_3(q^2) \right. \\
& \left. + \gamma_\mu \gamma_5 g_1(q^2) + i \sigma_{\mu\nu} \gamma_5 q^\nu g_2(q^2) + q^\mu \gamma_5 g_3(q^2) \right] u_{\Lambda_b}(p_{\Lambda_b}), \tag{2.5}
\end{aligned}$$

$$\begin{aligned}
\langle \Lambda(p_\Lambda) | \bar{s} i \sigma_{\mu\nu} q^\nu (1 + \gamma_5) b | \Lambda_b(p_{\Lambda_b}) \rangle = & \bar{u}_\Lambda(p_\Lambda) \left[\gamma_\mu f_1^T(q^2) + i \sigma_{\mu\nu} q^\nu f_2^T(q^2) + q^\mu f_3^T(q^2) \right. \\
& \left. + \gamma_\mu \gamma_5 g_1^T(q^2) + i \sigma_{\mu\nu} \gamma_5 q^\nu g_2^T(q^2) + q^\mu \gamma_5 g_3^T(q^2) \right] u_{\Lambda_b}(p_{\Lambda_b}), \tag{2.6}
\end{aligned}$$

$$\begin{aligned}
\langle \Lambda(p_\Lambda) | \bar{s} i \sigma_{\mu\nu} q^\nu (1 - \gamma_5) b | \Lambda_b(p_{\Lambda_b}) \rangle = \bar{u}_\Lambda(p_\Lambda) & \left[\gamma_\mu f_1^T(q^2) + i \sigma_{\mu\nu} q^\nu f_2^T(q^2) + q^\mu f_3^T(q^2) \right. \\
& \left. - \gamma_\mu \gamma_5 g_1^T(q^2) - i \sigma_{\mu\nu} \gamma_5 q^\nu g_2^T(q^2) - q^\mu \gamma_5 g_3^T(q^2) \right] u_{\Lambda_b}(p_{\Lambda_b}) ,
\end{aligned} \tag{2.7}$$

$$\begin{aligned}
\langle \Lambda(p_\Lambda) | \bar{s} (1 + \gamma_5) b | \Lambda_b(p_{\Lambda_b}) \rangle = \frac{1}{m_b} \bar{u}_\Lambda(p_\Lambda) & \left[\not{q} f_1(q^2) + i q^\mu \sigma_{\mu\nu} q^\nu f_2(q^2) + q^2 f_3(q^2) \right. \\
& \left. - \not{q} \gamma_5 g_1(q^2) - i q^\mu \sigma_{\mu\nu} \gamma_5 q^\nu g_2(q^2) - q^2 \gamma_5 g_3(q^2) \right] u_{\Lambda_b}(p_{\Lambda_b}) ,
\end{aligned} \tag{2.8}$$

and,

$$\begin{aligned}
\langle \Lambda(p_\Lambda) | \bar{s} (1 - \gamma_5) b | \Lambda_b(p_{\Lambda_b}) \rangle = \frac{1}{m_b} \bar{u}_\Lambda(p_\Lambda) & \left[\not{q} f_1(q^2) + i q^\mu \sigma_{\mu\nu} q^\nu f_2(q^2) + q^2 f_3(q^2) \right. \\
& \left. + \not{q} \gamma_5 g_1(q^2) + i q^\mu \sigma_{\mu\nu} \gamma_5 q^\nu g_2(q^2) + q^2 \gamma_5 g_3(q^2) \right] u_{\Lambda_b}(p_{\Lambda_b}) ,
\end{aligned} \tag{2.9}$$

where q^2 is the transformed momentum squared; and the u_{Λ_b} and u_Λ are spinors of the initial and final baryons. In the meantime, the $f_i^{(T)}$ and $g_i^{(T)}$ with $i = 1, 2$ and 3 are transition form factors.

Using the above transition matrix elements in terms of form factors, we find the supersymmetric amplitude as

$$\begin{aligned}
\mathcal{M}_{SUSY}^{\Lambda_b \rightarrow \Lambda \ell^+ \ell^-} = \frac{G_F \alpha_{em} V_{tb} V_{ts}^*}{2\sqrt{2}\pi} & \left\{ \left[\bar{u}_\Lambda(p_\Lambda) (\gamma_\mu [\mathcal{A}_1 R + \mathcal{B}_1 L] + i \sigma_{\mu\nu} q^\nu [\mathcal{A}_2 R + \mathcal{B}_2 L] + q^\mu [\mathcal{A}_3 R + \mathcal{B}_3 L]) u_{\Lambda_b}(p_{\Lambda_b}) \right] (\bar{\ell} \gamma^\mu \ell) \right. \\
+ & \left[\bar{u}_\Lambda(p_\Lambda) (\gamma_\mu [\mathcal{D}_1 R + \mathcal{E}_1 L] + i \sigma_{\mu\nu} q^\nu [\mathcal{D}_2 R + \mathcal{E}_2 L] + q^\mu [\mathcal{D}_3 R + \mathcal{E}_3 L]) u_{\Lambda_b}(p_{\Lambda_b}) \right] (\bar{\ell} \gamma^\mu \gamma_5 \ell) \\
+ & \left[\bar{u}_\Lambda(p_\Lambda) (\not{q} [\mathcal{G}_1 R + \mathcal{H}_1 L] + i q^\mu \sigma_{\mu\nu} q^\nu [\mathcal{G}_2 R + \mathcal{H}_2 L] + q^2 [\mathcal{G}_3 R + \mathcal{H}_3 L]) u_{\Lambda_b}(p_{\Lambda_b}) \right] (\bar{\ell} \ell) \\
+ & \left[\bar{u}_\Lambda(p_\Lambda) (\not{q} [\mathcal{K}_1 R + \mathcal{S}_1 L] + i q^\mu \sigma_{\mu\nu} q^\nu [\mathcal{K}_2 R + \mathcal{S}_2 L] + q^2 [\mathcal{K}_3 R + \mathcal{S}_3 L]) u_{\Lambda_b}(p_{\Lambda_b}) \right] (\bar{\ell} \gamma_5 \ell) \left. \right\} ,
\end{aligned} \tag{2.10}$$

where $R = (1 + \gamma_5)/2$ and $L = (1 - \gamma_5)/2$ and the calligraphic coefficients are found as

$$\begin{aligned}
\mathcal{A}_1 &= f_1 C_9^{eff+} - g_1 C_9^{eff-} - 2m_b \frac{1}{q^2} \left[f_1^T C_7^{eff+} + g_1^T C_7^{eff-} \right], \quad \mathcal{A}_2 = \mathcal{A}_1 (1 \rightarrow 2), \quad \mathcal{A}_3 = \mathcal{A}_1 (1 \rightarrow 3), \\
\mathcal{B}_1 &= f_1 C_9^{eff+} + g_1 C_9^{eff-} - 2m_b \frac{1}{q^2} \left[f_1^T C_7^{eff+} - g_1^T C_7^{eff-} \right], \quad \mathcal{B}_2 = \mathcal{B}_1 (1 \rightarrow 2), \quad \mathcal{B}_3 = \mathcal{B}_1 (1 \rightarrow 3), \\
\mathcal{D}_1 &= f_1 C_{10}^+ - g_1 C_{10}^-, \quad \mathcal{D}_2 = \mathcal{D}_1 (1 \rightarrow 2), \quad \mathcal{D}_3 = \mathcal{D}_1 (1 \rightarrow 3), \\
\mathcal{E}_1 &= f_1 C_{10}^+ + g_1 C_{10}^-, \quad \mathcal{E}_2 = \mathcal{E}_1 (1 \rightarrow 2), \quad \mathcal{E}_3 = \mathcal{E}_1 (1 \rightarrow 3), \\
\mathcal{G}_1 &= \frac{1}{m_b} \left[f_1 C_{Q_1}^+ - g_1 C_{Q_1}^- \right], \quad \mathcal{G}_2 = \mathcal{G}_1 (1 \rightarrow 2), \quad \mathcal{G}_3 = \mathcal{G}_1 (1 \rightarrow 3), \\
\mathcal{H}_1 &= \frac{1}{m_b} \left[f_1 C_{Q_1}^+ + g_1 C_{Q_1}^- \right], \quad \mathcal{H}_2 = \mathcal{H}_1 (1 \rightarrow 2), \quad \mathcal{H}_3 = \mathcal{H}_1 (1 \rightarrow 3), \\
\mathcal{K}_1 &= \frac{1}{m_b} \left[f_1 C_{Q_2}^+ - g_1 C_{Q_2}^- \right], \quad \mathcal{K}_2 = \mathcal{K}_1 (1 \rightarrow 2), \quad \mathcal{K}_3 = \mathcal{K}_1 (1 \rightarrow 3), \\
\mathcal{S}_1 &= \frac{1}{m_b} \left[f_1 C_{Q_2}^+ + g_1 C_{Q_2}^- \right], \quad \mathcal{S}_2 = \mathcal{S}_1 (1 \rightarrow 2), \quad \mathcal{S}_3 = \mathcal{S}_1 (1 \rightarrow 3),
\end{aligned} \tag{2.11}$$

with

$$\begin{aligned}
C_9^{eff+} &= C_9^{eff} + C_9'^{eff}, & C_9^{eff-} &= C_9^{eff} - C_9'^{eff}, \\
C_7^{eff+} &= C_7^{eff} + C_7'^{eff}, & C_7^{eff-} &= C_7^{eff} - C_7'^{eff}, \\
C_{10}^+ &= C_{10} + C_{10}', & C_{10}^- &= C_{10} - C_{10}', \\
C_{Q_1}^+ &= C_{Q_1} + C_{Q_1}', & C_{Q_1}^- &= C_{Q_1} - C_{Q_1}', \\
C_{Q_2}^+ &= C_{Q_2} + C_{Q_2}', & C_{Q_2}^- &= C_{Q_2} - C_{Q_2}'.
\end{aligned} \tag{2.12}$$

3 Differential decay rate, branching fraction and FBA

3.1 The differential decay rate

In this part, we calculate the differential decay rate for the decay channel under consideration. Using the aforementioned amplitude, we find the supersymmetric differential decay rate in terms of form factors in full theory as:

$$\frac{d^2\Gamma}{d\hat{s}dz}(z, \hat{s}) = \frac{G_F^2 \alpha_{em}^2 m_{\Lambda_b}}{16384\pi^5} |V_{tb}V_{ts}^*|^2 v \sqrt{\lambda(1, r, \hat{s})} \left[\mathcal{T}_0(\hat{s}) + \mathcal{T}_1(\hat{s})z + \mathcal{T}_2(\hat{s})z^2 \right], \quad (3.13)$$

where $\lambda = \lambda(1, r, \hat{s}) = (1 - r - \hat{s})^2 - 4r\hat{s}$ is the usual triangle function with $\hat{s} = q^2/m_{\Lambda_b}^2$, $r = m_\ell^2/m_{\Lambda_b}^2$ and $v = \sqrt{1 - \frac{4m_\ell^2}{q^2}}$. Here also $z = \cos\theta$ with θ is the angle between momenta of the lepton l^+ and the Λ_b in the center of mass of leptons. The calligraphic, $\mathcal{T}_0(\hat{s})$, $\mathcal{T}_1(\hat{s})$ and $\mathcal{T}_2(\hat{s})$ functions are obtained as:

$$\begin{aligned} \mathcal{T}_0(\hat{s}) = & 32m_\ell^2 m_{\Lambda_b}^4 \hat{s} (1 + r - \hat{s}) \left(|\mathcal{D}_3|^2 + |\mathcal{E}_3|^2 \right) \\ & + 64m_\ell^2 m_{\Lambda_b}^3 (1 - r - \hat{s}) \operatorname{Re} \left[\mathcal{D}_1^* \mathcal{E}_3 + \mathcal{D}_3 \mathcal{E}_1^* \right] \\ & + 64m_{\Lambda_b}^2 \sqrt{r} (6m_\ell^2 - m_{\Lambda_b}^2 \hat{s}) \operatorname{Re} \left[\mathcal{D}_1^* \mathcal{E}_1 \right] \\ & + 64m_\ell^2 m_{\Lambda_b}^3 \sqrt{r} \left\{ 2m_{\Lambda_b} \hat{s} \operatorname{Re} \left[\mathcal{D}_3^* \mathcal{E}_3 \right] + (1 - r + \hat{s}) \operatorname{Re} \left[\mathcal{D}_1^* \mathcal{D}_3 + \mathcal{E}_1^* \mathcal{E}_3 \right] \right\} \\ & + 32m_{\Lambda_b}^2 (2m_\ell^2 + m_{\Lambda_b}^2 \hat{s}) \left\{ (1 - r + \hat{s}) m_{\Lambda_b} \sqrt{r} \operatorname{Re} \left[\mathcal{A}_1^* \mathcal{A}_2 + \mathcal{B}_1^* \mathcal{B}_2 \right] \right. \\ & \left. - m_{\Lambda_b} (1 - r - \hat{s}) \operatorname{Re} \left[\mathcal{A}_1^* \mathcal{B}_2 + \mathcal{A}_2^* \mathcal{B}_1 \right] - 2\sqrt{r} \left(\operatorname{Re} \left[\mathcal{A}_1^* \mathcal{B}_1 \right] + m_{\Lambda_b}^2 \hat{s} \operatorname{Re} \left[\mathcal{A}_2^* \mathcal{B}_2 \right] \right) \right\} \end{aligned}$$

$$\begin{aligned}
& + 8m_{\Lambda_b}^2 \left\{ 4m_\ell^2(1+r-\hat{s}) + m_{\Lambda_b}^2 \left[(1-r)^2 - \hat{s}^2 \right] \right\} \left(|\mathcal{A}_1|^2 + |\mathcal{B}_1|^2 \right) \\
& + 8m_{\Lambda_b}^4 \left\{ 4m_\ell^2 \left[\lambda + (1+r-\hat{s})\hat{s} \right] + m_{\Lambda_b}^2 \hat{s} \left[(1-r)^2 - \hat{s}^2 \right] \right\} \left(|\mathcal{A}_2|^2 + |\mathcal{B}_2|^2 \right) \\
& - 8m_{\Lambda_b}^2 \left\{ 4m_\ell^2(1+r-\hat{s}) - m_{\Lambda_b}^2 \left[(1-r)^2 - \hat{s}^2 \right] \right\} \left(|\mathcal{D}_1|^2 + |\mathcal{E}_1|^2 \right) \\
& + 8m_{\Lambda_b}^5 \hat{s} v^2 \left\{ -8m_{\Lambda_b} \hat{s} \sqrt{r} \operatorname{Re} \left[\mathcal{D}_2^* \mathcal{E}_2 \right] + 4(1-r+\hat{s}) \sqrt{r} \operatorname{Re} \left[\mathcal{D}_1^* \mathcal{D}_2 + \mathcal{E}_1^* \mathcal{E}_2 \right] \right. \\
& \left. - 4(1-r-\hat{s}) \operatorname{Re} \left[\mathcal{D}_1^* \mathcal{E}_2 + \mathcal{D}_2^* \mathcal{E}_1 \right] + m_{\Lambda_b} \left[(1-r)^2 - \hat{s}^2 \right] \left(|\mathcal{D}_2|^2 + |\mathcal{E}_2|^2 \right) \right\} \\
& - 8m_{\Lambda_b}^4 \left\{ 4m_\ell \left[(1-r)^2 - \hat{s}(1+r) \right] \operatorname{Re} \left[\mathcal{D}_1^* \mathcal{K}_1 + \mathcal{E}_1^* \mathcal{S}_1 \right] \right. \\
& + (4m_\ell^2 - m_{\Lambda_b}^2 \hat{s}) \left[(1-r)^2 - \hat{s}(1+r) \right] \left(|\mathcal{G}_1|^2 + |\mathcal{H}_1|^2 \right) \\
& \left. + 4m_{\Lambda_b}^2 \sqrt{r} \hat{s}^2 (4m_\ell^2 - m_{\Lambda_b}^2 \hat{s}) \operatorname{Re} \left[\mathcal{G}_3^* \mathcal{H}_3 \right] \right\} \\
& - 8m_{\Lambda_b}^5 \hat{s} \left\{ 2\sqrt{r} (4m_\ell^2 - m_{\Lambda_b}^2 \hat{s}) (1-r+\hat{s}) \operatorname{Re} \left[\mathcal{G}_1^* \mathcal{G}_3 + \mathcal{H}_1^* \mathcal{H}_3 \right] \right. \\
& + 4m_\ell \sqrt{r} (1-r+\hat{s}) \operatorname{Re} \left[\mathcal{D}_1^* \mathcal{K}_3 + \mathcal{E}_1^* \mathcal{S}_3 + \mathcal{D}_3^* \mathcal{K}_1 + \mathcal{E}_3^* \mathcal{S}_1 \right] \\
& + 4m_\ell (1-r-\hat{s}) \operatorname{Re} \left[\mathcal{D}_1^* \mathcal{S}_3 + \mathcal{E}_1^* \mathcal{K}_3 + \mathcal{D}_3^* \mathcal{S}_1 + \mathcal{E}_3^* \mathcal{K}_1 \right] \\
& + 2(1-r-\hat{s}) (4m_\ell^2 - m_{\Lambda_b}^2 \hat{s}) \operatorname{Re} \left[\mathcal{G}_1^* \mathcal{H}_3 + \mathcal{H}_1^* \mathcal{G}_3 \right] \\
& \left. - m_{\Lambda_b} \left[(1-r)^2 - \hat{s}(1+r) \right] \left(|\mathcal{K}_1|^2 + |\mathcal{S}_1|^2 \right) \right\} \\
& - 32m_{\Lambda_b}^4 \sqrt{r} \hat{s} \left\{ 2m_\ell \operatorname{Re} \left[\mathcal{D}_1^* \mathcal{S}_1 + \mathcal{E}_1^* \mathcal{K}_1 \right] + (4m_\ell^2 - m_{\Lambda_b}^2 \hat{s}) \operatorname{Re} \left[\mathcal{G}_1^* \mathcal{H}_1 \right] \right\} \\
& + 8m_{\Lambda_b}^6 \hat{s}^2 \left\{ 4\sqrt{r} \operatorname{Re} \left[\mathcal{K}_1^* \mathcal{S}_1 \right] + 2m_{\Lambda_b} \sqrt{r} (1-r+\hat{s}) \operatorname{Re} \left[\mathcal{K}_1^* \mathcal{K}_3 + \mathcal{S}_1^* \mathcal{S}_3 \right] \right. \\
& + 2m_{\Lambda_b} (1-r-\hat{s}) \operatorname{Re} \left[\mathcal{K}_1^* \mathcal{S}_3 + \mathcal{S}_1^* \mathcal{K}_3 \right] \\
& - (4m_\ell^2 - m_{\Lambda_b}^2 \hat{s}) (1+r-\hat{s}) \left(|\mathcal{G}_3|^2 + |\mathcal{H}_3|^2 \right) \\
& \left. - 4m_\ell (1+r-\hat{s}) \operatorname{Re} \left[\mathcal{D}_3^* \mathcal{K}_3 + \mathcal{E}_3^* \mathcal{S}_3 \right] - 8m_\ell \sqrt{r} \operatorname{Re} \left[\mathcal{D}_3^* \mathcal{S}_3 + \mathcal{E}_3^* \mathcal{K}_3 \right] \right\} \\
& + 8m_{\Lambda_b}^8 \hat{s}^3 \left\{ (1+r-\hat{s}) \left(|\mathcal{K}_3|^2 + |\mathcal{S}_3|^2 \right) + 4\sqrt{r} \operatorname{Re} \left[\mathcal{K}_3^* \mathcal{S}_3 \right] \right\},
\end{aligned}$$

$$\begin{aligned}
\mathcal{T}_1(\hat{s}) = & -32m_{\Lambda_b}^4 m_\ell \sqrt{\lambda} v (1-r) \text{Re} \left(\mathcal{A}_1^* \mathcal{G}_1 + \mathcal{B}_1^* \mathcal{H}_1 \right) \\
& - 16m_{\Lambda_b}^4 \hat{s} v \sqrt{\lambda} \left\{ 2\text{Re} \left(\mathcal{A}_1^* \mathcal{D}_1 \right) - 2\text{Re} \left(\mathcal{B}_1^* \mathcal{E}_1 \right) \right. \\
& + 2m_{\Lambda_b} \text{Re} \left(\mathcal{B}_1^* \mathcal{D}_2 - \mathcal{B}_2^* \mathcal{D}_1 + \mathcal{A}_2^* \mathcal{E}_1 - \mathcal{A}_1^* \mathcal{E}_2 \right) \\
& + 2m_{\Lambda_b} m_\ell \text{Re} \left(\mathcal{A}_1^* \mathcal{H}_3 + \mathcal{B}_1^* \mathcal{G}_3 - \mathcal{A}_2^* \mathcal{H}_1 - \mathcal{B}_2^* \mathcal{G}_1 \right) \left. \vphantom{\frac{1}{2}} \right\} \\
& + 32m_{\Lambda_b}^5 \hat{s} v \sqrt{\lambda} \left\{ m_{\Lambda_b} (1-r) \text{Re} \left(\mathcal{A}_2^* \mathcal{D}_2 - \mathcal{B}_2^* \mathcal{E}_2 \right) \right. \\
& + \sqrt{r} \text{Re} \left(\mathcal{A}_2^* \mathcal{D}_1 + \mathcal{A}_1^* \mathcal{D}_2 - \mathcal{B}_2^* \mathcal{E}_1 - \mathcal{B}_1^* \mathcal{E}_2 \right) \\
& - \sqrt{r} m_\ell \text{Re} \left(\mathcal{A}_1^* \mathcal{G}_3 + \mathcal{B}_1^* \mathcal{H}_3 + \mathcal{A}_2^* \mathcal{G}_1 + \mathcal{B}_2^* \mathcal{H}_1 \right) \left. \vphantom{\frac{1}{2}} \right\} \\
& + 32m_{\Lambda_b}^6 m_\ell \sqrt{\lambda} v \hat{s}^2 \text{Re} \left(\mathcal{A}_2^* \mathcal{G}_3 + \mathcal{B}_2^* \mathcal{H}_3 \right),
\end{aligned} \tag{3.15}$$

$$\begin{aligned}
\mathcal{T}_2(\hat{s}) = & -8m_{\Lambda_b}^4 v^2 \lambda \left(|\mathcal{A}_1|^2 + |\mathcal{B}_1|^2 + |\mathcal{D}_1|^2 + |\mathcal{E}_1|^2 \right) \\
& + 8m_{\Lambda_b}^6 \hat{s} v^2 \lambda \left(|\mathcal{A}_2|^2 + |\mathcal{B}_2|^2 + |\mathcal{D}_2|^2 + |\mathcal{E}_2|^2 \right).
\end{aligned} \tag{3.16}$$

In order to obtain the differential decay rate only in terms of \hat{s} , we fulfill integrate Eq.(3.13) over z in the interval $[-1, 1]$. As a result, we get

$$\frac{d\Gamma}{d\hat{s}}(\hat{s}) = \frac{G_F^2 \alpha_{em}^2 m_{\Lambda_b}}{8192\pi^5} |V_{tb} V_{ts}^*|^2 v \sqrt{\lambda} \left[\mathcal{T}_0(\hat{s}) + \frac{1}{3} \mathcal{T}_2(\hat{s}) \right]. \tag{3.17}$$

3.2 The differential branching ratio

Using the differential decay rate, in this subsection, we numerically analyze the differential branching ratio and calculate the values of the branching ratios at different lepton channels. For this aim, we need sum inputs which we would like to present them here. In Table 1, we present the masses [9] as well as the lifetime of the initial baryon [9], some constants and elements of the CKM matrix.

The main inputs in our calculations are form factors. These form factors are calculated via light cone QCD sum rules in full theory in [10]. The fit function for the form factors

Some Input Parameters	Values
m_e	0.00051 <i>GeV</i>
m_μ	0.1056 <i>GeV</i>
m_τ	1.776 <i>GeV</i>
m_b	4.8 <i>GeV</i>
m_{Λ_b}	5.620 <i>GeV</i>
m_Λ	1.1156 <i>GeV</i>
τ_{Λ_b}	1.425×10^{-12} s
\hbar	6.582×10^{-25} <i>GeV s</i>
G_F	1.17×10^{-5} <i>GeV⁻²</i>
α_{em}	1/137
$ V_{tb}V_{ts}^* $	0.041

Table 1: The values of some input parameters used in the analysis.

$f_1, f_2, f_3, g_1, g_2, g_3, f_2^T, f_3^T, g_2^T$ and g_3^T is given as [10]:

$$f_i^{(T)}(q^2)[g_i^{(T)}(q^2)] = \frac{a}{\left(1 - \frac{q^2}{m_{fit}^2}\right)} + \frac{b}{\left(1 - \frac{q^2}{m_{fit}^2}\right)^2}, \quad (3.18)$$

where the fit parameters a , b and m_{fit}^2 as well as the values of the related form factors at $q^2 = 0$ in full theory are given in Table 2. Furthermore, the fit function of the form factors f_1^T and g_1^T is given by [10]:

$$f_1^T(q^2)[g_1^T(q^2)] = \frac{c}{\left(1 - \frac{q^2}{m_{fit}^{'2}}\right)} - \frac{c}{\left(1 - \frac{q^2}{m_{fit}^{''2}}\right)^2}, \quad (3.19)$$

where, the parameters c , $m_{fit}^{'2}$ and $m_{fit}^{''2}$ as well as the values of the corresponding form factors at $q^2 = 0$ are presented in Table 3.

In our numerical analysis, it is important to emphasize that the Wilson coefficient C_9^{eff} has been taken to contain also the long distance (LD) effects coming from the charmonium resonances. These effects are parameterized using the Breit-Weigner ansatz as [11–13]:

$$Y_{LD} = \frac{3\pi}{\alpha^2} C^{(0)} \sum_{i=1}^6 \kappa_i \frac{\Gamma(V_i \rightarrow \ell^+ \ell^-) m_{V_i}}{m_{V_i}^2 - q^2 - im_{V_i} \Gamma_{V_i}}, \quad (3.20)$$

where, $C^{(0)} = 0.362$ and κ_i are the phenomenological factors. Here, m_{V_i} and Γ_{V_i} are the masses and decay rates of the vector charmonia, respectively. In the present work,

	a	b	m_{fit}^2	form factors at $q^2 = 0$
f_1	-0.046	0.368	39.10	0.322 ± 0.112
f_2	0.0046	-0.017	26.37	-0.011 ± 0.004
f_3	0.006	-0.021	22.99	-0.015 ± 0.005
g_1	-0.220	0.538	48.70	0.318 ± 0.110
g_2	0.005	-0.018	26.93	-0.013 ± 0.004
g_3	0.035	-0.050	24.26	-0.014 ± 0.005
f_2^T	-0.131	0.426	45.70	0.295 ± 0.105
f_3^T	-0.046	0.102	28.31	0.056 ± 0.018
g_2^T	-0.369	0.664	59.37	0.294 ± 0.105
g_3^T	-0.026	-0.075	23.73	-0.101 ± 0.035

Table 2: The parameters in the fit function of the form factors $f_1, f_2, f_3, g_1, g_2, g_3, f_2^T, f_3^T, g_2^T$ and g_3^T as well as their values at $q^2 = 0$ in full theory [10].

	c	$m_{fit}'^2$	$m_{fit}''^2$	form factors at $q^2 = 0$
f_1^T	-1.191	23.81	59.96	0 ± 0.0
g_1^T	-0.653	24.15	48.52	0 ± 0.0

Table 3: The parameters in the fit function of the form factors f_1^T and g_1^T as well as their values at $q^2 = 0$ in full theory [10].

we only take into account the two lowest resonances that are $J/\psi(1s)$ and $\psi(2s)$. The phenomenological factors have also been chosen as $\kappa_1 \cong 1$ and $\kappa_2 \cong 2$. The masses, branching fractions and total decay widths related to the considered resonances are given in Table 4.

Family of J/ψ	$Mass[GeV]$	$\Gamma(V_i \rightarrow \ell^+ \ell^-)$	Γ_{V_i}
$J/\psi(1s)$	3.096	5.55×10^{-6}	92.9×10^{-6}
$\psi(2s)$	3.686	2.35×10^{-6}	304×10^{-6}

Table 4: The values of masses, branching fractions and total decay widths related to the resonances $J/\psi(1s)$ and $\psi(2s)$ [9].

Considering the above mentioned resonances from J/ψ family, we divide the allowed physical regions into the following three regions in the case of the electron and muon as

final leptons:

$$\begin{aligned}
\text{Region I} & \ ; \ 4m_l^2 \leq q^2 \leq (m_{J/\psi(1s)} - 0.02)^2, \\
\text{Region II} & \ ; \ (m_{J/\psi(1s)} + 0.02)^2 \leq q^2 \leq (m_{\psi(2s)} - 0.02)^2, \\
\text{Region III} & \ ; \ (m_{\psi(2s)} + 0.02)^2 \leq q^2 \leq (m_{\Lambda_b} - m_\Lambda)^2.
\end{aligned}$$

In the case of τ , we have the following two regions:

$$\begin{aligned}
\text{Region I} & \ ; \ 4m_\tau^2 \leq q^2 \leq (m_{\psi(2s)} - 0.02)^2, \\
\text{Region II} & \ ; \ (m_{\psi(2s)} + 0.02)^2 \leq q^2 \leq (m_{\Lambda_b} - m_\Lambda)^2.
\end{aligned}$$

Finally, we would like to present the numerical values of the Wilson coefficients used in numerical calculations in Table 5.

Coefficient	SM	SUSY I	SUSY II	SUSY III	SUSY SO(10)($A_0 = -1000$)
C_7^{eff}	-0.313	+0.376	+0.376	-0.376	-0.219
C_9^{eff}	4.334	4.767	4.767	4.767	4.275
C_{10}	-4.669	-3.735	-3.735	-3.735	-4.732
C_{Q_1}	0	0	6.5(16.5)	1.2(4.5)	$0.106 + 0i(1.775 + 0.002i)$
C_{Q_2}	0	0	-6.5(-16.5)	-1.2(-4.5)	$-0.107 + 0i(-1.797 - 0.002i)$
$C_7'^{eff}$	0	0	0	0	$0.039 + 0.038i$
$C_9'^{eff}$	0	0	0	0	$0.011 + 0.072i$
C_{10}'	0	0	0	0	$-0.075 - 0.67i$
C_{Q_1}'	0	0	0	0	$-0.247 + 0.242i(-4.148 + 4.074i)$
C_{Q_2}'	0	0	0	0	$-0.25 + 0.246i(-4.202 + 4.128i)$

Table 5: The Wilson coefficients used in numerical calculations [3, 4, 6, 14]. In the values containing parentheses, the values inside the parentheses stand for the τ lepton, while the values outside belong to the e and μ cases. The other values (without parentheses) refer to all leptons.

Having given all the inputs, we now present the dependence of the differential branching ratio on \hat{s} for the e , μ and τ leptons in the SM and different SUSY scenarios in Figures 1 and 2. From these figures which are plotted considering the central values of the form factors, we see that

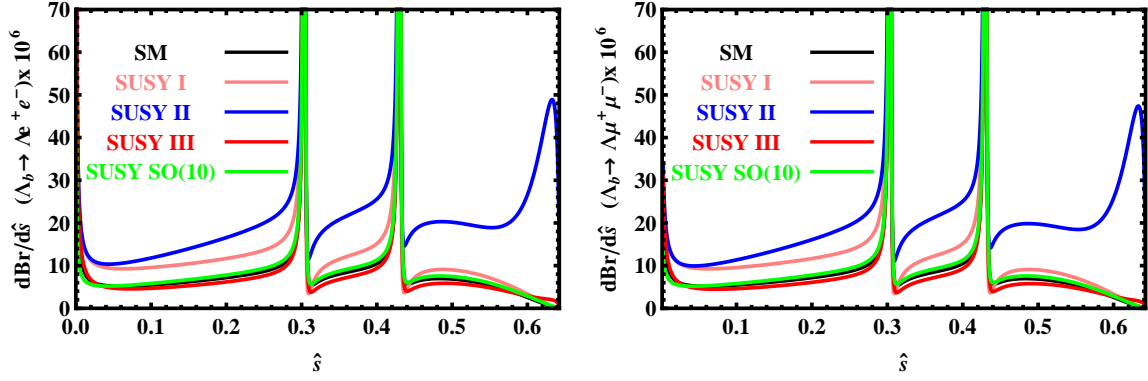


Figure 1: The dependence of the differential branching ratio on \hat{s} for the $\Lambda_b \rightarrow \Lambda e^+ e^-$ and $\Lambda_b \rightarrow \Lambda \mu^+ \mu^-$ transitions in SM and different SUSY models using the central values of form factors.

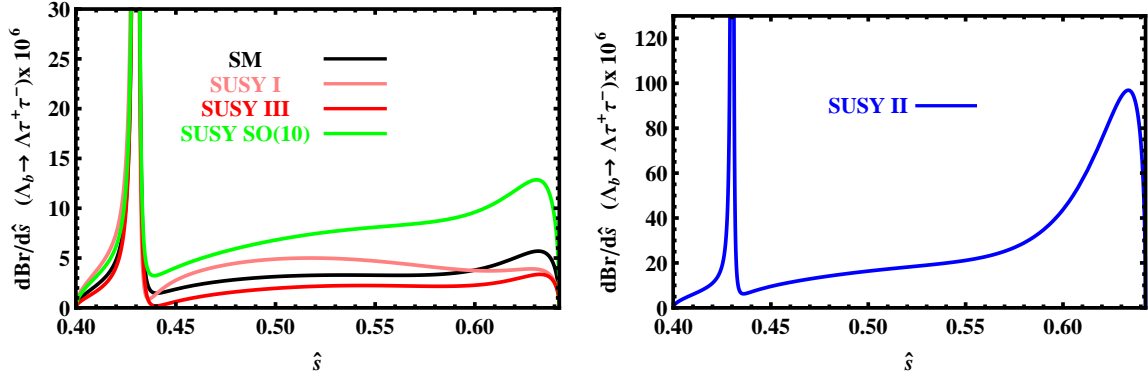


Figure 2: The dependence of the differential branching ratio on \hat{s} for the $\Lambda_b \rightarrow \Lambda \tau^+ \tau^-$ transition in SM and different SUSY models using the central values of form factors.

- in all lepton channels, the predictions of the SUSY II deviate maximally from those of the SM and other considered SUSY models. In the case of τ , this deviation reaches to approximately one order of magnitude.
- As far as the e and μ are concerned, the results obtained via the SUSY I have also considerable deviation from the predictions of the other models.
- In the case of τ as final lepton, we see sizable differences between all models' predictions. The nearest results to the SM correspond to the SUSY I and III.

$BR(\Lambda_b \rightarrow \Lambda e^+ e^-)$	<i>Region I</i>	<i>Region II</i>	<i>Region III</i>
SM	2.86×10^{-6}	1.12×10^{-6}	0.81×10^{-6}
SUSY I	4.57×10^{-6}	1.56×10^{-6}	0.99×10^{-6}
SUSY II	5.66×10^{-6}	2.69×10^{-6}	2.61×10^{-6}
SUSY III	2.93×10^{-6}	0.98×10^{-6}	0.66×10^{-6}
SUSY SO(10)	2.65×10^{-6}	1.20×10^{-6}	1.09×10^{-6}

Table 6: The central values of branching ratio for $\Lambda_b \rightarrow \Lambda e^+ e^-$ decay channel at different regions in SM and different SUSY models.

$BR(\Lambda_b \rightarrow \Lambda \mu^+ \mu^-)$	<i>Region I</i>	<i>Region II</i>	<i>Region III</i>
SM	2.25×10^{-6}	1.12×10^{-6}	0.81×10^{-6}
SUSY I	3.69×10^{-6}	1.56×10^{-6}	0.99×10^{-6}
SUSY II	4.65×10^{-6}	2.63×10^{-6}	2.55×10^{-6}
SUSY III	2.04×10^{-6}	0.97×10^{-6}	0.65×10^{-6}
SUSY SO(10)	2.33×10^{-6}	1.20×10^{-6}	1.09×10^{-6}

Table 7: The central values of branching ratio for $\Lambda_b \rightarrow \Lambda \mu^+ \mu^-$ decay channel at different regions in SM and different SUSY models.

3.3 The branching ratio

Integrating the differential branching ratio over \hat{s} in the considered regions and taking into account the central values of the form factors, we find the branching ratios for various models as presented in Tables 6, 7 and 8 for different lepton channels. A quick glance at these Tables leads to the following results:

- as it is expected the values of the branching ratio decrease when going from the e to τ .
- The order of branching ratios indicates that these channels are accessible at the LHC. Note that as we have already mentioned this decay channel has been observed by CDF Collaboration at Fermilab in μ channel [7].
- All SUSY models have predictions considerably different than those of the SM in all regions and at all lepton channels.
- The maximum deviation from the SM results belongs to the SUSY II model. When considering the numerical values, the maximum deviation of the SUSY II result from

$BR(\Lambda_b \rightarrow \Lambda \tau^+ \tau^-)$	<i>Region I</i>	<i>Region II</i>
SM	0.87×10^{-7}	3.84×10^{-7}
SUSY I	1.35×10^{-7}	5.55×10^{-7}
SUSY II	2.01×10^{-7}	2.44×10^{-6}
SUSY III	0.72×10^{-7}	2.13×10^{-7}
SUSY SO(10)	1.12×10^{-7}	1.61×10^{-6}

Table 8: The central values of branching ratio for $\Lambda_b \rightarrow \Lambda \tau^+ \tau^-$ decay channel at different regions in SM and different SUSY models.

the SM prediction corresponds to the region II for τ channel. In this case, the result of the SUSY II is approximately 6 times greater than that of the SM.

3.4 The FBA

The lepton forward-backward asymmetry (\mathcal{A}_{FB}) is defined as:

$$\mathcal{A}_{FB} = \frac{N_f - N_b}{N_f + N_b}. \quad (3.21)$$

where N_f is the number of moving particles to forward direction and N_b is the number of moving particles to backward direction. In technique language, the lepton FBA is written in terms of the differential decay rate as:

$$\mathcal{A}_{FB}(\hat{s}) = \frac{\int_0^1 \frac{d^2\Gamma}{d\hat{s}dz}(z, \hat{s}) dz - \int_{-1}^0 \frac{d^2\Gamma}{d\hat{s}dz}(z, \hat{s}) dz}{\int_0^1 \frac{d^2\Gamma}{d\hat{s}dz}(z, \hat{s}) dz + \int_{-1}^0 \frac{d^2\Gamma}{d\hat{s}dz}(z, \hat{s}) dz}. \quad (3.22)$$

Using this definition, we plot the dependence of the lepton FBA on \hat{s} for e , μ and τ channels in the SM and different SUSY models in Figures 3 and 4. From these figures which are also plotted considering the central values of the form factors, it is clear that,

- in the case of the e and μ channels, the SUSY I and II behave different than the other models. In these channels for the small values of the \hat{s} , the maximum deviation belongs to the SUSY I, however, for higher values of the \hat{s} the maximum deviation corresponds to the SUSY II.
- In τ channel, the maximum deviation from the SM prediction belongs to the SUSY III.

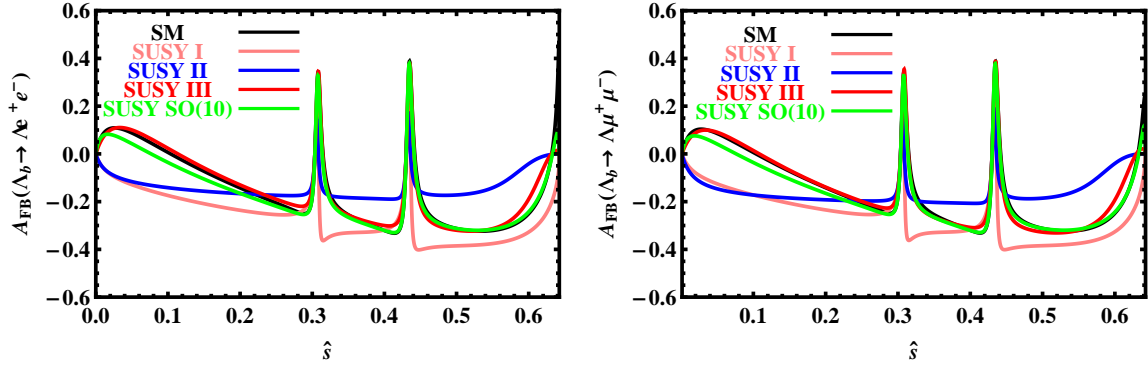


Figure 3: The dependence of the FBA on \hat{s} for $\Lambda_b \rightarrow \Lambda e^+ e^-$ and $\Lambda_b \rightarrow \Lambda \mu^+ \mu^-$ transitions in SM and different SUSY scenarios using the central values of form factors.

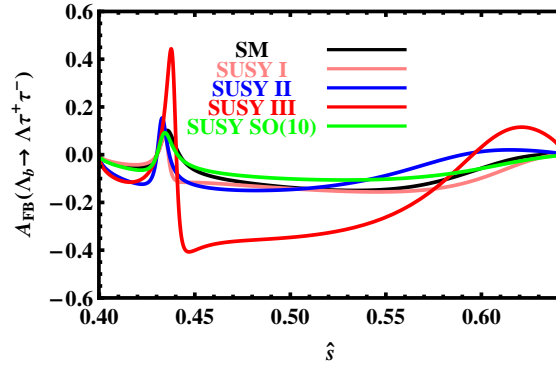


Figure 4: The dependence of the FBA on \hat{s} for $\Lambda_b \rightarrow \Lambda \tau^+ \tau^-$ transition in SM and different SUSY scenarios using the central values of form factors.

- The zero points of the FBA in different SUSY models move slightly to the left compare to the SM predictions. In some regions, the SUSY I, II and III have different signs with the SM predictions.
- The SUSY SO(10) represents overall the closest results to the SM predictions.

3.5 The physical quantities under consideration taking into account the uncertainties of the form factors

In this subsection, we would like to consider the above mentioned physical quantities taking into account the uncertainties of the form factors and discuss the effects of these errors on the results. For this aim, considering the errors of the form factors, we plot the dependence of the differential branching ratio and FBA on \hat{s} at different lepton channels and different models in figures 5-8. From these figures we see that,

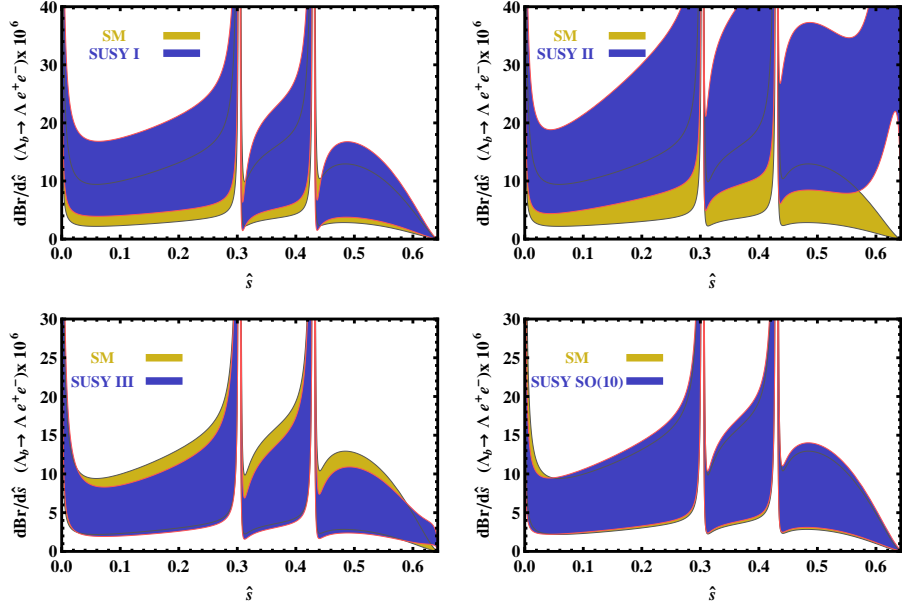


Figure 5: Comparison of the results of differential branching ratio with respect to \hat{s} for the $\Lambda_b \rightarrow \Lambda e^+ e^-$ transition obtained from different SUSY models with that of the SM considering the errors of form factors.

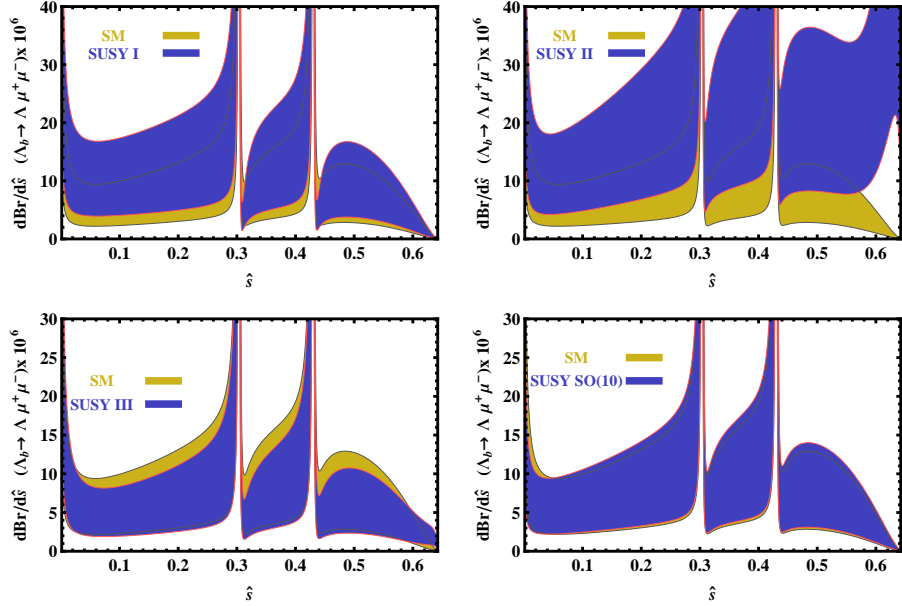


Figure 6: The same as Figure 5 but for μ .

- as far as the differential branching ratio are concerned, at the e and μ channels, the band of SUSY SO(10) approximately covers the band of the SM. In the case of the SUSY I, II and III, although their bands coincide with that of the SM, there are some regions that these SUSY models have different predictions. Among these different

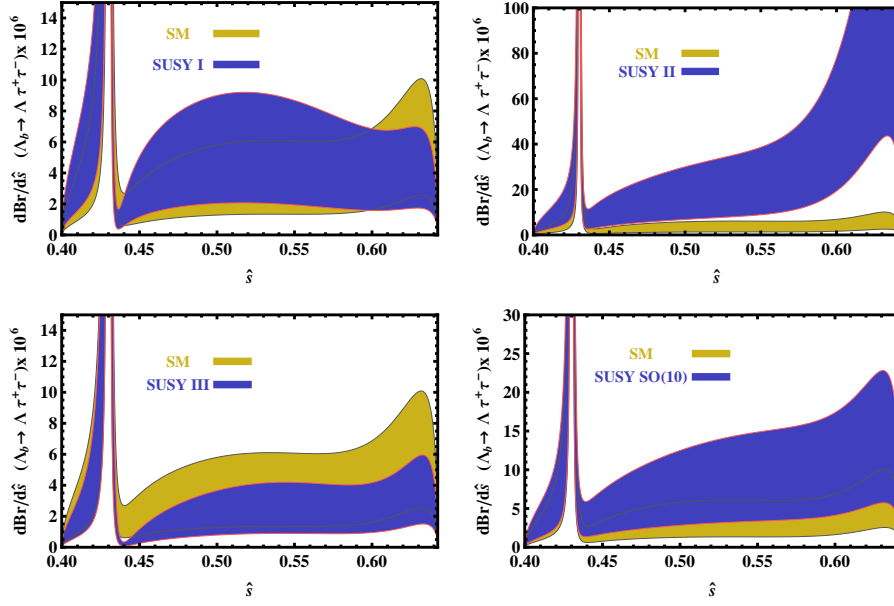


Figure 7: The same as Figure 5 but for τ .

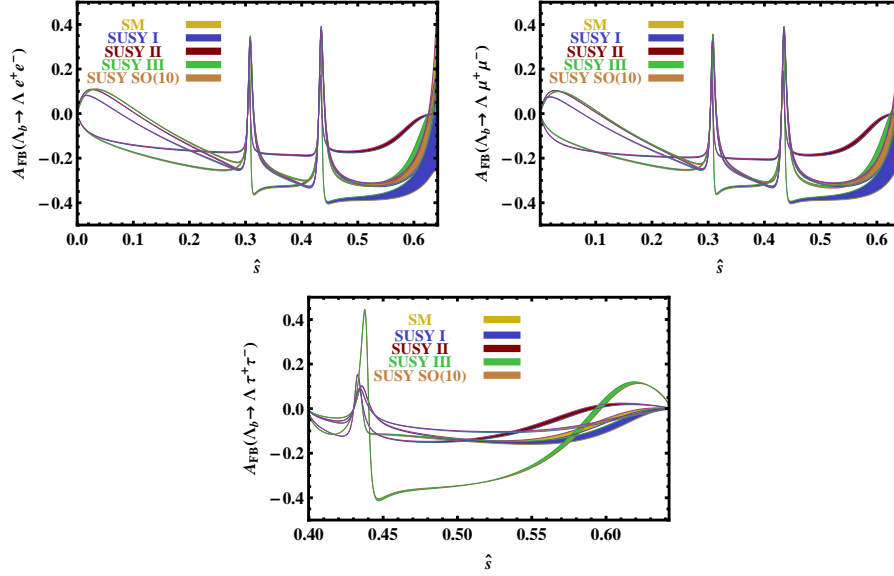


Figure 8: Comparison of the results of the FBA with respect to \hat{s} for all lepton channels obtained from different SUSY models with that of the SM considering the errors of form factors.

SUSY models, the maximum discrepancy from the SM prediction belongs to the SUSY II. In τ channel, the difference between different SUSY models predictions and that of the SM can not be completely killed by the errors of form factors for any SUSY models. In this channel, there are also common regions between the bands of SUSY models and that of the SM, except than the SUSY II which does not approximately

$BR(\Lambda_b \rightarrow \Lambda e^+ e^-)$	<i>Region I</i>	<i>Region II</i>	<i>Region III</i>
SM	$(2.86 \pm 1.43) \times 10^{-6}$	$(1.12 \pm 0.56) \times 10^{-6}$	$(0.81 \pm 0.40) \times 10^{-6}$
SUSY I	$(4.57 \pm 2.42) \times 10^{-6}$	$(1.56 \pm 0.82) \times 10^{-6}$	$(0.99 \pm 0.52) \times 10^{-6}$
SUSY II	$(5.66 \pm 3.05) \times 10^{-6}$	$(2.69 \pm 1.45) \times 10^{-6}$	$(2.61 \pm 1.40) \times 10^{-6}$
SUSY III	$(2.93 \pm 1.52) \times 10^{-6}$	$(0.98 \pm 0.50) \times 10^{-6}$	$(0.66 \pm 0.34) \times 10^{-6}$
SUSY SO(10)	$(2.65 \pm 1.35) \times 10^{-6}$	$(1.20 \pm 0.61) \times 10^{-6}$	$(1.09 \pm 0.55) \times 10^{-6}$

Table 9: The values of branching ratio for $\Lambda_b \rightarrow \Lambda e^+ e^-$ decay channel at different regions in SM and different SUSY models considering the uncertainties of form factors.

$BR(\Lambda_b \rightarrow \Lambda \mu^+ \mu^-)$	<i>Region I</i>	<i>Region II</i>	<i>Region III</i>
SM	$(2.25 \pm 1.12) \times 10^{-6}$	$(1.12 \pm 0.56) \times 10^{-6}$	$(0.81 \pm 0.40) \times 10^{-6}$
SUSY I	$(3.69 \pm 1.95) \times 10^{-6}$	$(1.56 \pm 0.82) \times 10^{-6}$	$(0.99 \pm 0.52) \times 10^{-6}$
SUSY II	$(4.65 \pm 2.51) \times 10^{-6}$	$(2.63 \pm 1.42) \times 10^{-6}$	$(2.55 \pm 1.37) \times 10^{-6}$
SUSY III	$(2.04 \pm 1.06) \times 10^{-6}$	$(0.97 \pm 0.50) \times 10^{-6}$	$(0.65 \pm 0.33) \times 10^{-6}$
SUSY SO(10)	$(2.33 \pm 1.18) \times 10^{-6}$	$(1.20 \pm 0.61) \times 10^{-6}$	$(1.09 \pm 0.55) \times 10^{-6}$

Table 10: The values of branching ratio for $\Lambda_b \rightarrow \Lambda \mu^+ \mu^-$ decay channel at different regions in SM and different SUSY models considering the uncertainties of form factors.

coincide anywhere with the SM result.

- In the case of the FBA, the errors of form factors do not approximately affect the central values, except than the higher values of \hat{s} , which we see narrow bands for different SUSY models as well as the SM. At e and μ channels, the bands of the SUSY I, SUSY III, SUSY SO(10) and SM coincide with each other somewhere at higher values of \hat{s} , but the SUSY II has different prediction. At τ channel, all models have different predictions.
- As it is expected, the forward-backward asymmetry and in particular its zero-crossing points are more robust than the differential branching ratio such that they are not approximately affected by the uncertainties of the form factors. This is the case also in $B \rightarrow K^{(*)} l^+ l^-$ channel.

Now, we discuss the effects of the uncertainties of the form factors for the branching ratios at different regions and for different models. Taking into account the errors of form factors, we present the values of branching ratios at different channels in Tables 9, 10 and 11. From these Tables we deduce the same results as we have seen from the

$BR(\Lambda_b \rightarrow \Lambda \tau^+ \tau^-)$	<i>Region I</i>	<i>Region II</i>
SM	$(0.87 \pm 0.43) \times 10^{-7}$	$(3.84 \pm 1.92) \times 10^{-7}$
SUSY I	$(1.35 \pm 0.71) \times 10^{-7}$	$(5.55 \pm 2.94) \times 10^{-7}$
SUSY II	$(2.01 \pm 1.08) \times 10^{-7}$	$(2.44 \pm 1.31) \times 10^{-6}$
SUSY III	$(0.72 \pm 0.37) \times 10^{-7}$	$(2.13 \pm 1.10) \times 10^{-7}$
SUSY SO(10)	$(1.12 \pm 0.57) \times 10^{-7}$	$(1.61 \pm 0.82) \times 10^{-6}$

Table 11: The values of branching ratio for $\Lambda_b \rightarrow \Lambda \tau^+ \tau^-$ decay channel at different regions in SM and different SUSY models considering the uncertainties of form factors.

figures of the differential branching ratio. Although the central values for different SUSY models and the SM differ considerably from each other, considering the errors of the presented results in these Tables, we observe that approximately in all cases the results of different models coincide with each other, except for the SUSY II and SUSY SO(10) at τ channel and region II which have considerable discrepancy with the other model predictions.

4 Conclusion

In the present work, we have calculated the amplitude and differential decay rate for the semileptonic $\Lambda_b \rightarrow \Lambda \ell^+ \ell^-$ transition in different supersymmetric models. We have taken into account all twelve form factors entered the low energy matrix elements and recently calculated via light cone QCD sum rules in full theory to analyze the differential branching ratio, total branching fraction and the lepton forward-backward asymmetry. We have considered different SUSY scenarios in the calculations and compared the obtained results with the SM predictions. As far as the central values of the form factors are considered, in general, we observed considerable deviations from the SM predictions. In the case of the (differential) branching ratio, the maximum deviations from the SM predictions belong to the SUSY II scenario. As far as the FBA is concerned, at e and μ channels and lower values of the \hat{s} , the maximum deviation belongs to the SUSY I, however, for the higher values of the \hat{s} and the same lepton channels, the maximum discrepancy corresponds again to the SUSY II model. Taking into account the uncertainties of the form factors, we have observed that the branching ratio is more affected by these errors. The bands of the SUSY SO(10) approximately cover the SM bands at the e and μ channels. For other SUSY models and all lepton channels, although we have seen some intersection regions between different

SUSY bands and the SM predictions, there are considerable discrepancies between the SM and SUSY models predictions. Especially, at τ channel, there is a big discrepancy between the SUSY II and the SM bands. When we consider the FBA, the uncertainties of the form factors do not affect this quantity and its zero-crossing points. We see overall a considerable discrepancies between the narrow bands of the different considered SUSY models and that of the SM. Such discrepancies can be considered as a signal for existence of the supersymmetric particles.

The orders of the branching ratio at all lepton channels and all the considered regions of q^2 depict that these decay channels can be checked at LHC in near future. Note that as we have also previously stressed, this channel for μ case has been observed recently by CDF Collaboration at Fermilab. We are waiting for the LHCb Collaboration results on these channels, which they have in their physics program [8].

Comparison of the experimental results on the branching ratio as well as the FBA with the predictions of the present work, especially determination of the sign and zero-crossing points of the FBA, which have not been affected by the errors of the form factors, can help us get valuable information about the existence of the SUSY particles.

As we have already noticed, in numerical analysis, we have used the values of the Wilson coefficients presented in Table 5 for different SUSY scenarios. These values are obtained when the masses of the neutral Higgs bosons are taken in the interval $(91 - 200) \text{ GeV}$ (see for instance [4, 15–17]). Considering the recent developments by the CMS and ATLAS Collaborations at CERN on the mass of the Higgs-like boson ($\sim 125 \text{ GeV}$), the used values of the Wilson coefficients are still viable. However, after clarifying whether the obtained boson at LHC is the standard or non-standard Higgs, and using its exact mass, one may recalculate the Wilson coefficients in different SUSY scenarios. Obviously, it will be possible to improve the obtained results in the present work using the new values of the Wilson coefficients.

References

- [1] J. Incandela, CMS talk at “Latest update in the search for the Higgs boson at CERN”, July 4, 2012; F. Gianotti, ATLAS talk at “Latest update in the search for the Higgs boson at CERN”, July 4, 2012.
- [2] M. Hirsch, F. R. Joaquim, A. Vicente, “Constrained SUSY seesaws with a 125 GeV Higgs” [arXiv:1207.6635 [hep-ph]].

- [3] Q.-Sh. Yan, Ch.-Sh. Huang, L. Wei, Sh.-H. Zhu, “Exclusive Semileptonic Rare Decays $B \rightarrow (K, K^*)\ell^+\ell^-$ in Supersymmetric Theories”, Phys. Rev. D **62**, 094023 (2000) [arXiv:hep-ph/0004262].
- [4] W.-J. Li, Y.-B. Dai, Ch.-Sh. Huang, “Exclusive Semileptonic Rare Decays $B \rightarrow K^{(*)}\ell^+\ell^-$ in a SUSY SO(10) GUT”, Eur. Phys. J. C **40**, 565 (2005) [arXiv:hep-ph/0410317].
- [5] M. J. Aslam, Y.-M. Wang, C.-D. Lü, “Exclusive semileptonic decays of $\Lambda_b \rightarrow \Lambda\ell^+\ell^-$ in supersymmetric theories”, Phys. Rev. D **78**, 114032 (2008) [arXiv:0808.2113 [hep-ph]].
- [6] A. Ahmed, I. Ahmed, M. A. Paracha, M. Junaid, A. Rehman, M. J. Aslam, “Comparative Study of $B_c \rightarrow D_s^*\ell^+\ell^-$ Decays in Standard Model and Supersymmetric Models” [arXiv:1108.1058 [hep-ph]].
- [7] T. Aaltonen *et al.* [CDF Collaboration], “Observation of the Baryonic Flavor-Changing Neutral Current Decay $\Lambda_b^0 \rightarrow \Lambda\mu^+\mu^-$ ”, Phys. Rev. Lett. **107**, 201802 (2011) [arXiv:1107.3753 [hep-ex]].
- [8] Our personal communications with Yasmine Sara Amhis from LHCb Collaboration.
- [9] J. Beringer et al. (Particle Data Group), Phys. Rev. D **86**, 010001 (2012).
- [10] T. M. Aliev, K. Azizi, M. Savci, “Analysis of the $\Lambda_b \rightarrow \Lambda\ell^+\ell^-$ decay in QCD”, Phys. Rev. D **81**, 056006 (2010) [arXiv:1001.0227 [hep-ph]].
- [11] G. Buchalla, A. J. Buras, M. E. Lautenbacher, “Weak decays beyond leading logarithms”, Rev. Mod. Phys. **68**, 1125 (1996) [arXiv:hep-ph/9512380].
- [12] M. Beneke, G. Buchalla, M. Neubert, C. T. Sachrajda, “Penguins with charm and quarkhadron duality”, Eur. Phys. J. C **61**, 439 (2009) [arXiv:0902.4446 [hep-ph]].
- [13] A. Khodjamirian, Th. Mannel, A.A. Pivovarov, Y.-M. Wang, “Charm-loop effect in $B \rightarrow K^{(*)}\ell^+\ell^-$ and $B \rightarrow K^*\gamma$ ”, JHEP **1009**, 089 (2010) [arXiv:1006.4945 [hep-ph]].
- [14] M. J. Aslam, C.-D. Lu, Y.-M. Wang, “ $B \rightarrow K_0^*(1430)\ell^+\ell^-$ decays in supersymmetric theories”, Phys. Rev. D **79**, 074007 (2009) [arXiv:0902.0432 [hep-ph]].
- [15] J.-F. Cheng, Ch.-Sh. Huang, X.-H. Wu, “Neutral Higgs boson contributions to CP asymmetry of $B \rightarrow \Phi K_S$ in MSSM”, Phys. Lett. B **585**, 287 (2004) [arXiv:hep-ph/0306086].

- [16] Ch.-Sh. Huang, P. Ko, X.-H. Wu, Y.-D. Yang, “MSSM Anatomy of the Polarization Puzzle in $B \rightarrow \phi K^*$ Decays”, Phys. Rev. D **73**, 034026 (2006) [arXiv:hep-ph/0511129].
- [17] J.-F. Cheng, Ch.-Sh. Huang, X.-H. Wu, “CP asymmetries in $B \rightarrow \phi K_S$ and $B \rightarrow \eta' K_S$ in MSSM”, Nucl. Phys. B **701**, 54 (2004) [arXiv:hep-ph/0404055].